arTs Università degli Studi di Trieste
Archivio della ricerca – postprint

Toward the Understanding of the Structure–Activity Correlation in Single-Site Mn Covalent Organic Frameworks for Electrocatalytic CO_2 Reduction

Geyla C. Dubed Bandomo, Federico Franco, Changwei Liu, Suvendu Sekhar Mondal, Angelo Gallo, Carlo Nervi, and Julio Lloret-Fillol*

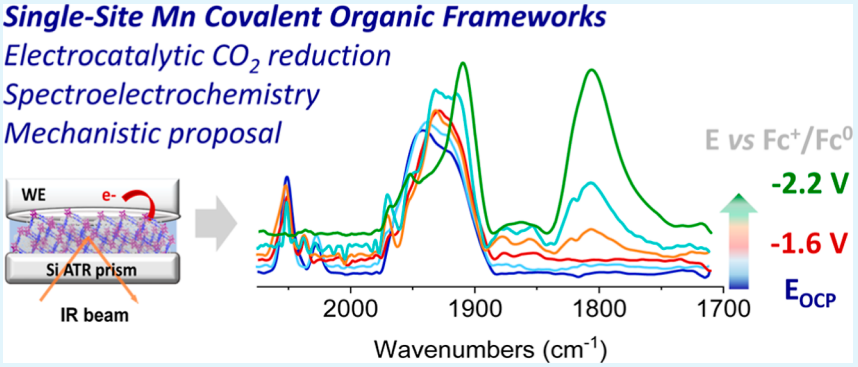

ABSTRACT: The encapsulation of organometallic complexes into reticular covalent organic frameworks (COFs) represents an effective strategy for the immobilization of molecular electrocatalysts. In particular, well-defined polypyridyl Mn sites embedded into a crystalline COF backbone ($\mathbf{COF_{bpyMn}}$) were found to exhibit higher selectivity and activity toward electrochemical CO_2 reduction compared to the parent molecular derivative noncovalently immobilized on carbon electrodes. In situ mechanistic studies revealed that the electronic and steric features of the reticular framework strongly affect the redox mechanism of the Mn sites, stabilizing the formation of a mononuclear Mn(I) radical anion intermediate over the most common off-cycle Mn^0–Mn^0 dimer. Herein, we report the study of a Mn-based COF ($\mathbf{COF_{PTMn}}$), introducing a larger phenanthroline building block, to explore how tuning the structural and electronic properties of the lattice may affect the catalytic CO_2 reduction performance and the mechanism at the molecular level of the reticular system. The Mn sites encapsulated into the reticular $\mathbf{COF_{PTMn}}$ exhibited a remarkable enhancement in the intrinsic catalytic CO_2 reduction activity at near-neutral pH compared to that of the corresponding noncovalently immobilized molecular derivative. On the other hand, the poor crystallinity and porosity of $\mathbf{COF_{PTMn}}$, likely introduced by the lattice expansion and spatial dynamics of the phenanthroline linker, were found to limit its catalytic performances compared to those of the bipyridyl $\mathbf{COF_{bpyMn}}$ analogue. ATR-IR spectroelectrochemistry revealed that the higher spatial mobility of the Mn sites does not completely suppress the Mn^0–Mn^0 dimerization upon the electrochemical reduction of the Mn sites at the $\mathbf{COF_{bpyMn}}$. This work highlights the positive role of the reticular structure of the material in enhancing its catalytic activity versus that of its molecular counterpart and provides useful hints for the future design and development of efficient reticular frameworks for electrocatalytic applications.

KEYWORDS: *CO_2 reduction, single atom catalysis, covalent organic framework, structure–activity relationship, spectroelectrochemistry, mechanisms*

INTRODUCTION

Incorporating catalytic units into reticular frameworks is an attractive strategy to maximize the number of active sites supported on an electrode and enhance the electrocatalytic activity compared with that of solution-based molecular electrocatalysts and other monolayer immobilization strategies.[1−12] In addition, the molecular design of covalent organic frameworks (COFs) allows outstanding control over the chemical environment of the catalytic sites in confined spaces with the aim to stabilize key reaction intermediates and control the activity and selectivity of catalytic processes. Several efforts have been oriented toward the rational design of COFs by

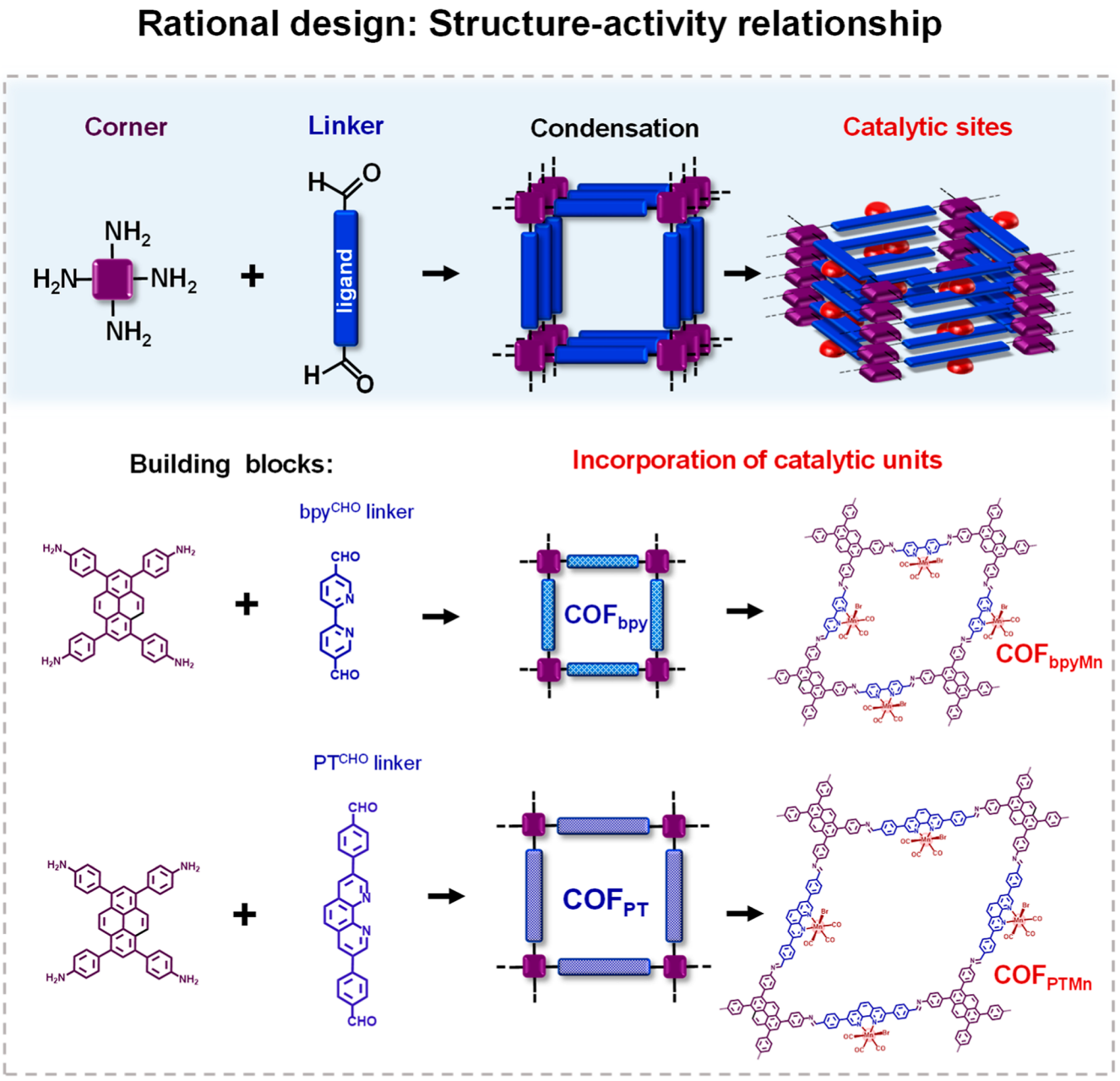

Figure 1. Modular reticular design of COFs by the modification of the polypyridyl linkers.

varying the size, shape, connectivity, and electronic structures of their molecular building blocks.[2,4,7,13−34] In particular, tuning the electronic structure of the building blocks can strongly influence the COF performance, mimicking the crucial role of ligands in molecular catalysis.

In the field of electrocatalytic reduction of CO_2 to value-added chemicals, extensive work has been focused on catalyst incorporation to tune the catalytic performances of reticular systems.[1,35−38] Yaghi and co-workers have demonstrated the ability to tune the CO_2 reduction properties of catalytic sites located at the corners of a COF by modifying the electronic properties of the linkers, indicating that a long-range electronic effect can efficiently promote the tuning of catalytic properties.[6] Bipyridines have also proven to be functional building blocks for COFs in electrocatalysis, similarly to porphyrins.[39−41] For example, Marinescu and co-workers evaluated a COF with both metalloporphyrin (Co and Fe) and metal bipyridine (Re) moieties for electrocatalytic CO_2 reduction, highlighting the effect of building blocks on the electrocatalytic properties of COFs and the importance of studying the catalytic activity−structure relationships of these reticular materials.[41]

These findings demonstrate the potential of reticular materials as efficient and selective electrocatalysts for CO_2 reduction. However, the precise mechanisms behind these catalytic processes and the structure−activity relationships governing their performances are not yet well understood. Further research is needed to fully elucidate these fundamental correlations and develop even more effective catalytic materials.

Recently, we have reported the encapsulation of {*fac*-$Mn(CO)_3$} molecular moieties into a reticular 2D imine-linked COF with bipyridyl ligands (**COF_{bpyMn}**) as an effective strategy to enhance the electrocatalytic activity and selectivity of the prototypical *fac*-$Mn(bpy)(CO)_3Br$ molecular catalyst for the CO_2 reduction to CO in an aqueous electrolyte.[2] This study

Scheme 1. Synthetic Procedure of COF_{PT} and COF_{PTMn}

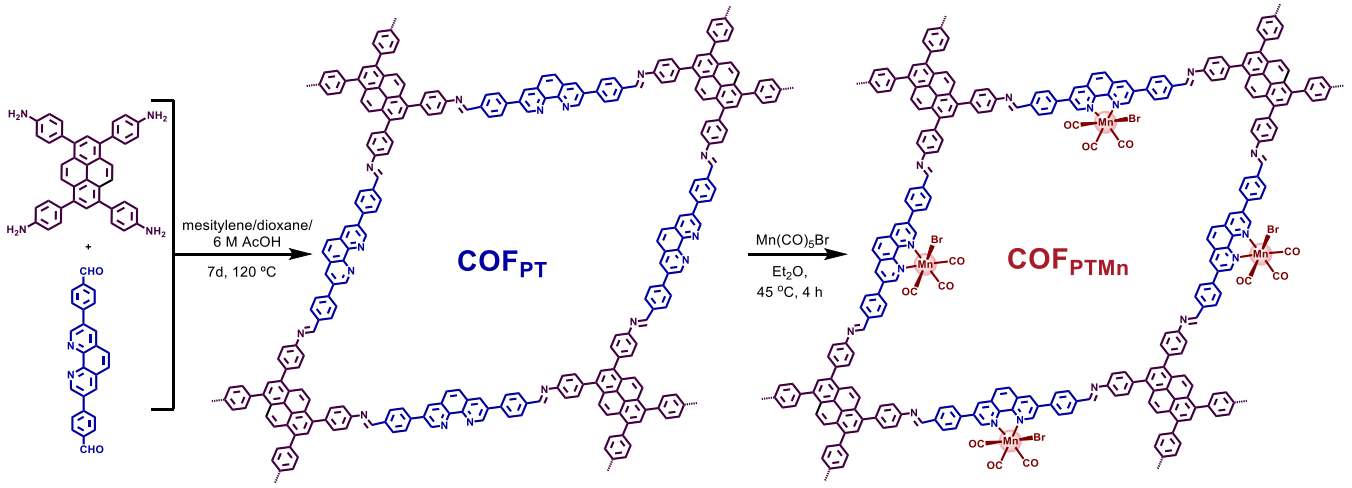

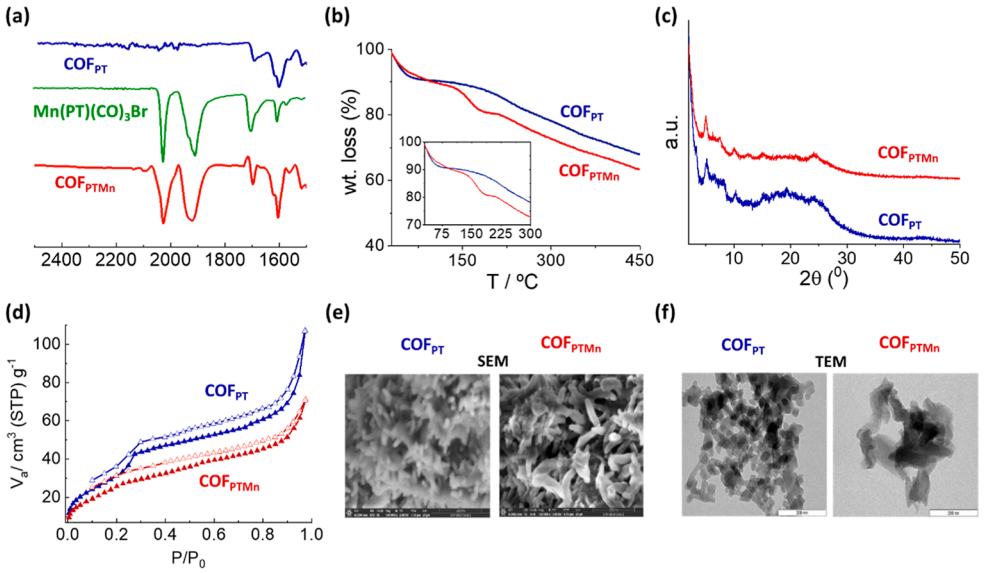

Figure 2. Characterization of COF_{PT} and COF_{PTMn}: (a) ATR-FT-IR spectra; (b) TGA; (c) PXRD; (d) N_2 absorption/desorption isotherms at 77 K; (e) FESEM images; and (f) TEM images.

provides insights into how the extended π-conjugated character and structural properties of reticular materials can be used to enhance their electrocatalytic performance. Compared to the molecular parent complex noncovalently immobilized on carbon electrodes, the highly crystalline and porous COF_{bpyMn} catalyst showed superior CO_2 reduction activity and selectivity while sterically suppressing the Mn^0—Mn^0 reductive dimerization typically occurring in nonreticular heterogenized molecular Mn counterparts. ATR-IR spectroelectrochemistry (SEC) studies showed that the formation of isolated Mn sites in COF_{bpyMn} contributes to the stabilization of a mononuclear, singly reduced intermediate.

In this context, we aimed to investigate the impact of structural modifications on the electrocatalytic properties of COFs by replacing the bipyridyl linker of COF_{bpyMn} with a 1,10-phenanthroline-based moiety bearing phenyl substituents at the 3,8 positions (4,4′-(1,10-phenanthroline-3,8-diyl)-dibenzaldehyde, PT^{CHO}) (Figure 1). The resulting COF_{PTMn} material was thoroughly characterized and evaluated for electrocatalytic CO_2 reduction in near-neutral pH in aqueous media. While COF_{PTMn} shows enhanced intrinsic catalytic CO_2 reduction activity compared to that of the nonreticular immobilized *fac*-$Mn(PT^{CHO})(CO)_3Br$ counterpart (Mn^{PT}), the comparison of COF_{PTMn} with COF_{bpyMn} provides insights into the correlation between structural aspects of reticular systems, such as lattice expansion and crystallinity, and their catalytic activity. Furthermore, ATR-IR SEC was used to investigate the catalytic mechanism of COF_{PTMn}, revealing that the expanded phenanthroline derivative influences the intermediates generated during the catalytic cycle. This work contributes to the understanding of how the reticular structure affects the CO_2 reduction performances. Moreover, results obtained by ATR-IR-SEC show the importance of developing new analytical tools and techniques to probe the complex behavior of reticular materials under reaction conditions.

RESULTS AND DISCUSSION

Synthesis and Characterization of COF_{PT} and COF_{PTMn}. The 2D COF_{PT} was synthesized following an already reported procedure[2,42] based on the two-component condensation between a terminal tetraamine (4,4′,4″,4‴-(pyrene-1,3,6,8-tetrayl)tetraaniline (PyTTA)) and a dialdehyde (4,4′-(1,10-

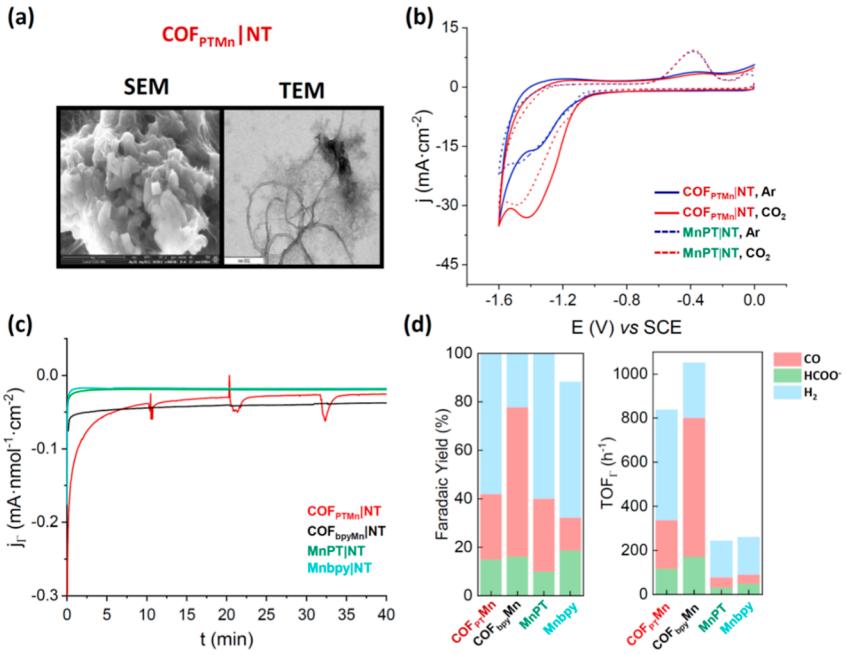

Figure 3. (a) FESEM and TEM of **COF_{PTMn}|NT**; (b) cyclic voltammograms on GC of **COF_{PTMn}|NT** ($[Mn]_{total}$ = 900 nmol·cm^{-2}, solid line) and **Mn^{PT}|NT** ($[Mn]_{total}$ = 900 nmol·cm^{-2}, dotted line) in water ($NaHCO_3$ 0.5 M) under Ar (blue, pH 8.4) and CO_2 (red, pH 7.4) at 100 mV·s^{-1}. (c) CPEs of **COF_{PTMn}|NT**, **COF_{bpyMn}|NT**, **Mn_{bpy}**, and **Mn^{PT}|NT** on CP (1 cm^2) at −1.34 V vs SCE (−0.67 V vs RHE) under CO_2 in water ($NaHCO_3$ 0.5 M, pH 7.4). (d) Faradaic yields and TOF_Γ. Generated products: CO (pink), $HCOO^-$ (green), and H_2 (blue).

phenanthroline-3,8-diyl)dibenzaldehyde) linker (PT^{CHO}, see Supporting Information for details, Scheme 1).[43] The Mn sites were introduced into **COF_{PT}** by postfunctionalization. **COF_{PT}** was reacted with $Mn(CO)_5Br$ at 45 °C for 4 h in diethyl ether, yielding a dark orange microcrystalline powder, namely, **COF_{PTMn}**.

The ATR-FT-IR spectrum of **COF_{PTMn}** shows the incorporation of $\{Mn(CO)_3Br\}$ moieties into the **COF_{PT}** backbone in a *fac* coordination geometry, exhibiting two prominent CO stretching frequencies at 2027 and 1922 cm^{-1}, which match the ones of the homologous $Mn(PT)(CO)_3Br$ (**Mn^{PT}**) complex (Figure 2a). The CO stretching values for **COF_{PTMn}** are also very similar to those previously reported for **COF_{bpyMn}** (Figure S10).[2] Thermogravimetric analysis (TGA) of **COF_{PTMn}** displays two decomposition steps at ∼70−180 and ∼200−900 °C, respectively (Figure 2b). The former is likely due to the thermal release of the CO ligands bound to the Mn centers, while the one occurring at higher temperatures could be assigned to decomposition. The TGA profile of **COF_{PT}** displays a single continuous material decomposition step.

The powder X-ray diffraction (PXRD) pattern of **COF_{PTMn}** shows diffraction peaks in the region between *ca.* 5 and 30°, matching the pattern of the as-synthesized **COF_{PT}** (Figure 2c). This suggests that the framework maintains its crystalline integrity even after metalation (Figure 2c). Nevertheless, the lower intensity of the Bragg peaks and the ill-defined character of the PXRD patterns of both **COF_{PT}** and **COF_{PTMn}** indicate less crystalline character compared to those of recently reported analogous bipyridyl-based COFs (Figure S11).[2] Such a difference in crystallinity may be related to COF formation and growth, which decrease with potential nonplanar conformations of linkers as the $\pi-\pi$ stacking interaction between interlayers strongly influences the COF formation rate.[44−46] In the case of **COF_{PT}**, the PT^{CHO} linker planarity is disrupted due to the free rotation of the phenyl ring, thus hindering the formation of a crystalline reticular framework.[44] In addition, the ^{13}C CP-MAS solid-state NMR spectra of the COFs show broad peaks as expected for the amorphous frameworks (Figure S12).

In addition to crystallinity, the structural features of the molecular building block also affect the porosity of the reticular material. The nitrogen (N_2) absorption/desorption isotherms (77 K) of **COF_{PT}** and **COF_{PTMn}** (Figure 2d) indicate indeed that the materials present low porosity with Brunauer−Emmett−Teller (BET) surface areas determined to be 130 and 94 m^2/g, respectively. The remarkable difference between the surface areas of **COF_{PT}** (130 m^2/g) and the previously evaluated **COF_{bpy}** (2127 m^2/g) represents a clear indicator of the modification of the structural properties of the COF because of the ligand modification, mainly due to the bigger size and the nonplanarity of the PT^{CHO} linker.

The amount of Mn incorporated within **COF_{PT}** was estimated by ICP-OES to be 38 mg/g, corresponding to the metalation of *ca.* 36% of the phenanthroline moieties available in the material. We ascribe the relatively low incorporation of Mn in **COF_{PTMn}** to the low crystallinity of the material, in which the presence of amorphous and irregular channels reduces the accessibility of binding sites within the pores. In this regard, high crystallinity helps to increase the accessible surface area and pore volume of the COFs, exposing more well-ordered binding sites.[47] Additionally, field emission scanning electron microscopy (FESEM) and transmission electron microscopy (TEM) images of **COF_{PT}** and **COF_{PTMn}** reveal that the materials tend to form particles of *ca.* 500 nm size with tubular morphologies (Figures 2e,f).

Electrocatalytic CO_2 Reduction in Aqueous Near-Neutral pH. The electrochemical behavior and the catalytic CO_2 reduction performances of **COF_{PTMn}** were explored in an aqueous 0.5 M $NaHCO_3$ electrolyte. For the electrode preparation, **COF_{PTMn}** was supported on a carbon electrode by drop-casting a dispersion of the catalyst powder, MWCNTs (NT) and Nafion (**COF_{PTMn}|NT**) (see Supporting Information

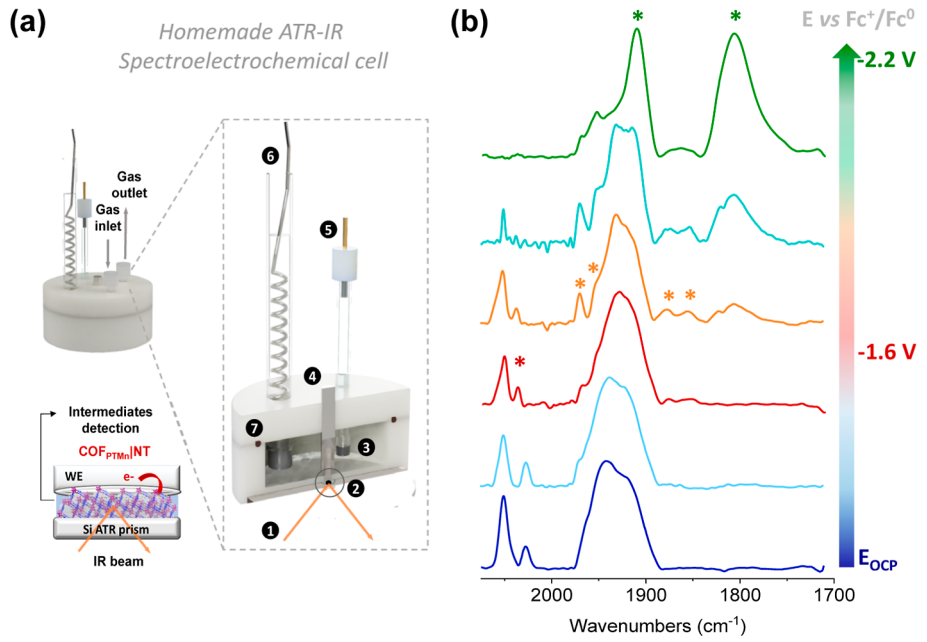

Figure 4. (a) Schematic representation of the ATR-IR-SEC cell (see Supporting Information for details) and (b) ATR-SEC of **COF$_{PTMn}$|NT** showing the precatalyst (blue spectrum), the first reduction process to form a contribution of the radical intermediate $[Mn^{I}L^{\bullet-}(S)]^0$ (red asterisk) and the dimer $[Mn^0L]_2$ (orange asterisks), and the second reduction process to form the anion five-coordinate intermediate $[MnL]^-$ (green asterisks). All spectra were recorded in CH_3CN (0.2 M $TBAPF_6$) under Ar.

for details). FESEM images of the functionalized electrode show a uniform distribution of **COF$_{PTMn}$** and NTs on the electrode surface (Figure 3a). The electrochemistry of **COF$_{PTMn}$|NT** was studied against the molecular counterpart Mn(PT)(CO)$_3$Br, supported by noncovalently $\pi-\pi$ stacking interaction on NTs (**Mn^{PT}|NT**).

Under Ar (pH 8.4), the cyclic voltammetry (CV) of **COF$_{PTMn}$|NT** shows an irreversible cathodic wave (full blue lines in Figure 3b) at an onset potential of −1.0 V vs SCE, analogous to that observed for **Mn^{PT}|NT** (dashed blue lines, Figure 3b), describing the reduction of the electroactive immobilized diimine Mn^I centers. The observed current density also accounts for a partial contribution due to the catalytic H_2 evolution reaction (HER), as confirmed by electrolysis experiments (vide infra). On the reverse scan, **Mn^{PT}|NT** displays an intense reoxidation peak at −0.38 V vs SCE, related to the oxidative cleavage of a Mn^0−Mn^0 dimer species formed upon the cathodic forward potential sweep.[48,49] Albeit lower in intensity, this feature is also apparent for **COF$_{PTMn}$|NT**. The lower intensity of this redox wave for **COF$_{PTMn}$|NT** may suggest a partial mechanical constraint of the Mn centers caused by the framework hindering Mn−Mn dimerization (vide infra).[2] When the electrolyte is saturated with CO_2 (pH ∼ 7.4), a 2-fold increase of the catalytic current is observed at −1.40 V vs SCE (−0.72 V vs RHE) for **COF$_{PTMn}$|NT**, which indicates a CO_2 electroreduction activity. This current increase is higher than the one shown by the noncovalent **Mn^{PT}|NT** electrode (Figure 3b, red curves).

For controlled-potential electrolysis (CPE), the **COF$_{PTMn}$|NT** and **Mn^{PT}|NT** catalysts were drop-casted on carbon paper (CP) (see Supporting Information for details, Figure 3a). For **COF$_{PTMn}$|NT**, the overall faradaic efficiency (FE) for CO_2 reduction products at −1.34 vs SCE (η = 550 mV, −0.67 V vs RHE) is 45% with CO as the predominant product (FE_{CO} = 30%) and minor $HCOO^-$ production (FE_{HCOO^-} = 15%), whereas the remaining charge accounts for HER (Figure 3c,d). In a similar manner, **Mn^{PT}|NT** produces *ca.* 30 and 10% of CO and $HCOO^-$, respectively (Figure 3d).

However, the electroactive surface concentrations (Γ, see Supporting Information for details) of **COF$_{PTMn}$|NT** and **Mn^{PT}|NT** were estimated to be ∼4 and 10% of the total Mn deposited, respectively (Figure S19). Normalizing the observed turnover frequency for Γ (TOF_Γ), the sum of the TOF_Γ values for CO and $HCOO^-$ formation at −1.34 V vs SCE (−0.67 V vs RHE) is 3-fold higher for **COF$_{PTMn}$|NT** than those for **Mn^{PT}|NT** (242 and 77 h^{-1}, respectively) (Figure 3d). This indicates that the Mn centers in the reticulated material are intrinsically more active than those in the molecular parent complex noncovalently functionalized over carbon electrodes, clearly highlighting the superior performances of the reticular system. A similar increase of catalyst activities has also been observed in the case of the covalent immobilization of Mn(bpy)-type complexes on carbon electrodes.[50,51]

In order to rationalize the structural effect of the molecular building blocks on CO_2 reduction catalysis of COFs, we compared the catalytic performances of **COF$_{PTMn}$|NT** with those of the reported analogue **COF$_{bpyMn}$|NT** (obtained with the bpy^{CHO} linker instead of the longer one PT^{CHO}, Figure 3c,d).[2] Both parent molecular complexes noncovalently functionalized over carbon electrodes (**Mn^{PT}|NT** and **Mn$_{bpy}$|NT**) exhibited similar catalytic performance in terms of either current density or selectivity (Figure 3c,d). Interestingly, the electronic and steric differences in the ligand framework have negligible effects on catalysis at the molecular level. On the other hand, the reticular **COF$_{bpyMn}$|NT** outperforms **COF$_{PTMn}$|NT**, providing a 2-fold higher overall current density and about an 8-fold enhancement in the molar yield of CO_2 reduction products (77 vs 10 μmol·cm^{-2} CO, Figure 3c,d). Moreover, the selectivity of **COF$_{bpyMn}$|NT** (S_{CO_2/H_2} = 3.5, see Supporting Information for details) toward CO_2 reduction over HER is higher than the one obtained with **COF$_{PTMn}$|NT** ($S_{CO_2/H2}$ = 0.6) at −1.34 V vs SCE

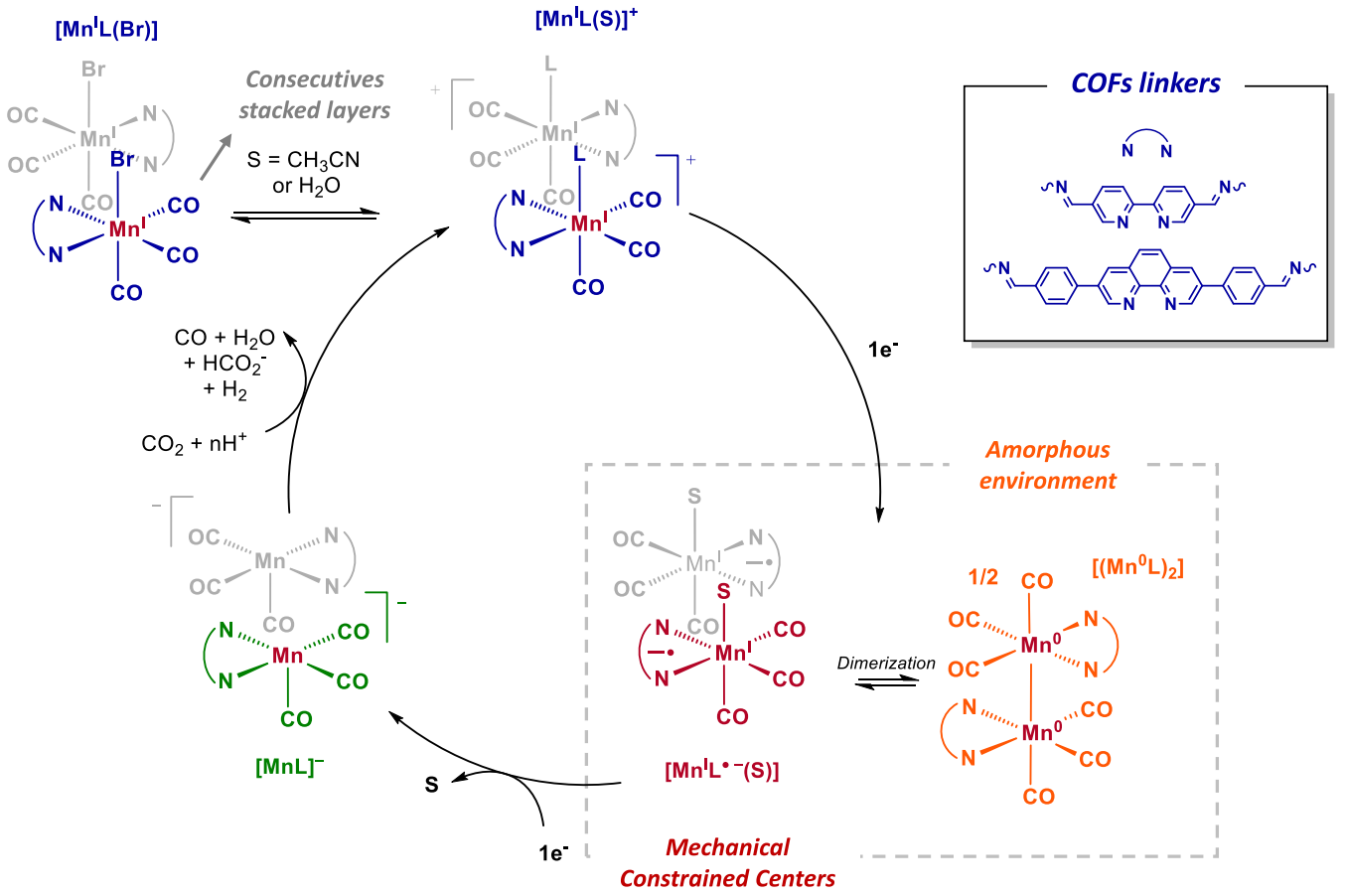

Figure 5. Proposed intermediates for $\mathbf{COF_{PTMn}}$ are based on spectroelectrochemical evidence.

(−0.67 V vs RHE) in a near-neutral electrolyte. Even considering the higher Mn incorporation and electroactive surface coverage (Γ_{Mn}) in $\mathbf{COF_{bpyMn}|NT}$ compared to that in $\mathbf{COF_{PTMn}|NT}$, the former still shows superior performances, resulting in a 3-fold higher normalized TOF_Γ for CO production (Figure 3d).

These results suggest that the structural properties of the molecular building blocks could be critical for the efficiency and selectivity of the electrocatalytic CO_2 reduction of reticular materials. Indeed, crystallinity reflects the porous structure's regularity, which is vital for electrical and mass transport phenomena.[52] The poor crystallinity and porosity of $\mathbf{COF_{PTMn}}$ could limit the electroactive Mn sites and hinder the accessibility of the substrate at the catalytic sites due to stacking faults or amorphous regions. In contrast, in highly porous and crystalline $\mathbf{COF_{bpyMn}}$, the self-assembled π-stacked columns enable electronic transport across the layers[53] and can favor substrate diffusion, thus increasing the local CO_2 concentration within the framework pores. On the other hand, as we mentioned above, $\mathbf{COF_{PTMn}}$ still shows superior catalytic performances compared to those of the noncovalently immobilized $\mathbf{Mn^{PT}|NT}$, showing significantly higher intrinsic activity of the single Mn sites. Our analysis suggests that differences in crystallinity likely influence the catalytic activity of COFs. However, this remains a hypothesis. The potential impacts of lattice expansion and ligand variations on modifying the electronic structure and, consequently, the catalysis cannot be entirely ruled out. Nonetheless, CV and SEC analyses of the $\mathbf{Mn^{bpy}}$ molecular catalyst in a homogeneous solution indicate that ligand substitution from bipyridine to phenanthroline does affect catalysis at the molecular level. However, these effects are relatively minor compared to those observed in COFs (Figure S23).

After a 1 h CPE at −1.34 vs SCE (−0.67 V vs RHE), no significant changes were observed for $\mathbf{COF_{PTMn}|NT}$ in terms of morphology and elemental composition by FESEM and energy dispersive X-ray (EDX) analysis (Figure S21a,b). Furthermore, the Mn coordination in $\mathbf{COF_{PTMn}}$ is also preserved after the catalytic test, as confirmed by ATR-IR (Figure S21c), showing the characteristic ν(CO) of {*fac*-Mn(CO)$_3$S} (S = Br, CH_3CN, and H_2O). However, ICP-OES of the electrolyte after CPE indicates that 5 to 18% of the total amount of Mn of the $\mathbf{COF_{PTMn}|NT}$ electrode leached out (Table S3).[2] Both the reduction in the ATR-IR intensity and the amount of Mn leaching can explain a part of the decrease of catalytic activity.

ATR-IR Spectroelectrochemistry. ATR-IR SEC was carried out on $\mathbf{COF_{PTMn}|NT}$ to investigate the effect of the structural properties of the reticular framework on the molecular intermediate species involved in the redox mechanism of the COF systems. The experiments were conducted by using a homemade ATR-IR spectroelectrochemical cell recently used for the study of analogous systems (see Supporting Information, Figure 4a).[2] Due to the concomitant catalytic HER observed for $\mathbf{COF_{PTMn}|NT}$ at low overpotentials in the near-neutral electrolyte, we performed the ATR-IR-SEC measurements in an anhydrous organic electrolyte (0.2 M $TBAPF_6$/MeCN). In these conditions, the cyclic voltammogram of $\mathbf{COF_{PTMn}|NT}$ under Ar shows two cathodic one-electron ($1e^-$) waves at −1.50 and −1.90 V vs $Fc^{+/0}$ (Figure S22), respectively, in agreement

with the voltammetric profile obtained for the homogeneous **Mn^{PT}** complex (Figure S23).

During the SEC experiments, the potential was decreased stepwise under Ar from the open-circuit potential (E_{OCP}) to −2.3 V vs $Fc^{+/0}$ to monitor the redox pathway of **COF$_{PTMn}$|NT** (Figure 4b). At E_{OCP}, the ATR spectrum of **COF$_{PTMn}$|NT** shows two ν(CO) bands at 2053 and 2028 cm^{-1} as well as a broad feature at 1937 cm^{-1}. This represents the mixture of two $\{Mn^{I}(CO)_3\}$ species in the *fac* arrangement containing axial Br^- or a neutral solvent molecule coordinated to Mn due to a solvolysis equilibrium.[48,49,54,55] Analogous species are also observed in the E_{OCP} spectrum recorded for the **Mn^{PT}|NT** electrode (Figure S24). Furthermore, the values of the ν(CO) stretches for **COF$_{PTMn}$|NT** are similar to those observed for **COF$_{bpyMn}$|NT**, suggesting a similar electronic Mn environment in both reticular systems.

Upon the first reduction wave, the decrease in the ν(CO) bands at 2053 and 2028 cm^{-1} of **COF$_{PTMn}$|NT** is accompanied by the growth of a new peak at 2037 cm^{-1} and a slight shift of the peak at 1943 cm^{-1} to lower energies. Analogous behavior was recently reported for **COF$_{bpyMn}$|NT** and was rationalized due to the formation of neutral $[Mn^{I}L^{\bullet-}(S)]$ radical species within the COF (Figure 4b).[2] Nevertheless, unlike the bipyridyl derivative, a new pattern of four new ν(CO) stretching modes at 1968, 1931, 1876, and 1854 cm^{-1} is apparent at an applied bias of *ca.* −1.8 V vs $Fc^{+/0}$ (Figure 4b). These bands are consistent with the formation of a Mn^0−Mn^0 dimeric species, similarly to the typical behavior reported for homogeneous tricarbonyl Mn complexes with diimine ligands.[56] The characteristic bands of the dimer tend to decrease at further negative applied potentials, with concurrent growth of two new ν(CO) stretches at 1910 and 1807 cm^{-1}, corresponding to the formation of the five-coordinate $[MnL]^-$ anionic species, well-known to be the active catalyst for CO_2-to-CO electroreduction (Figure 5, Table S4).[56,57] For the homogeneous prototypical bipyridyl Mn complex, it has been recently proposed that the dimeric species is primarily formed via an initial two-electron reduction of the Mn^{I} moiety, followed by a fast chemical parent−child reaction between the resulting Mn anion and the initial neutral Mn^{I} species.[58] This dimerization pathway is also consistent with the simultaneous observation of $[MnL]_2$, $[MnL]^-$, and the starting Mn^{I} species under reductive SEC of **COF$_{PTMn}$|NT** (Figure 4b, orange and light green spectra), indicating the mobility of Mn moieties in the NT environment.

For comparison, we performed ATR-SEC on the nonreticular **Mn^{PT}|NT** catalyst under the same conditions (Figure S24). As expected, the first reduction event was associated with the formation of the Mn^0−Mn^0 dimeric species,[56] with no evidence of radical formation. The ν(CO) bands of the dimer match well with those observed upon SEC reduction of the reticular **COF$_{PTMn}$|NT** counterpart. Moreover, the characteristic pattern of the five-coordinate $[MnL]^-$ anion (1906 and 1802 cm^{-1}) appears to grow at *ca.* −2.3 V vs $Fc^{+/0}$.

For noncovalent immobilization of Mn molecular complexes with diimine ligands, the Mn^0−Mn^0 dimeric species is the observed intermediate upon the first reduction event starting from the Mn^{I} complex. On the other hand, the encapsulation of Mn bipyridyl units into the highly crystalline and porous **COF$_{bpyMn}$** structure suppresses dimerization and stabilizes the mononuclear $[Mn^{I}L^{\bullet-}(S)]^0$ radical species due to both the electronic and steric effects of the reticular framework.[2] In the case of **COF$_{PTMn}$**, the embedded molecular Mn sites are only partially constrained by the lattice due to the poor crystallinity and porosity of the COF scaffold, leading to a mixture of mononuclear and dimeric species upon reduction of the original Mn^{I} moieties. We hypothesize that the introduction of the larger and nonplanar PT^{CHO} linker results in a partially amorphous environment of the Mn-diimine centers, thus increasing the mobility of the Mn sites.

The voltammetric data of **COF$_{PTMn}$|NT** are also consistent with this interpretation, displaying an oxidative wave at −0.35 V vs SCE (0.33 V vs RHE) upon the backward scan, which is assigned to the reoxidation of the Mn^0−Mn^0 dimer formed during the forward scan (Figure 3b).[2] This diagnostic peak appears to be very intense for the noncovalently functionalized **Mn^{PT}** complex (**Mn^{PT}|NT**) (Figure 3b), whereas it is almost absent in the cyclic voltammograms of the fully crystalline **COF$_{bpyMn}$|NT** (Figures S23 and S26).[2]

The proposed reductive mechanism of **COF$_{PTMn}$** is summarized in Figure 5. The initial Mn^{I} centers undergo a two-electron uptake at *ca.* −1.50 V vs $Fc^{+/0}$, leading to a mixture of the lattice-bound mononuclear anion $[Mn^{I}L^{\bullet-}(S)]^-$ and dimeric neutral Mn^0−Mn^0 species. While the charge delocalization effect of the COF structure is similar to the previously reported **COF$_{bpyMn}$** system,[2] the more amorphous character of the **COF$_{PTMn}$** framework induces a higher mobility of the single Mn sites, thus favoring a partial Mn^0−Mn^0 dimerization upon reduction. Further reduction of the dimeric species ultimately results in the formation of the five-coordinate $[MnL]^-$ anion, which is the catalytic species reacting with CO_2 and water to produce CO and $HCOO^-$.

CONCLUSIONS

In this work, we followed a modular reticular approach to synthesize a novel imine-based COF derived by the condensation between a pyrene tetraamine linker and the phenanthroline PT^{CHO} structure. The postsynthetic COF modification ultimately results in the formation of **COF$_{PTMn}$**, in which the Mn sites show an equivalent coordination Mn environment to the homologous molecular complex **Mn^{PT}**. **COF$_{PTMn}$** was found to be an active electrocatalyst for CO_2 reduction in a near-neutral pH aqueous electrolyte, leading to the formation of CO as the predominant product (FE_{CO} = 30%) and minor $HCOO^-$ production (FE_{HCOO^-} = 15%). Albeit the catalytic selectivity of **COF$_{PTMn}$** is similar to the one observed for the parent **Mn^{PT}** complex noncovalently immobilized on carbon electrodes, the Mn sites embedded into the reticular **COF$_{PTMn}$** framework are 3-fold more active than their molecular counterparts. The comparison between the catalytic performances of **COF$_{PTMn}$** and the previously reported bipyridyl **COF$_{bpyMn}$** analogue showed a structure−activity relationship. We hypothesized that the lattice expansion from **COF$_{bpyMn}$** to **COF$_{PTMn}$** could be responsible for the reduced crystallinity, catalytic activity, and selectivity, with **COF$_{bpyMn}$** being about 3-fold higher in CO_2 reduction activity than **COF$_{PTMn}$**.

Additionally, by ATR-SEC, two different intermediates were detected upon the first reduction of **COF$_{PTMn}$**: the $[Mn^{I}L^{\bullet-}(S)]^-$ radical anion and the $(Mn^{0}L)_2$ dimeric species. These results suggest a direct effect of the mechanical properties of the reticular platform on the mechanism of CO_2 reduction. Therefore, the disorder between the layers of **COF$_{PTMn}$** reduces the mechanical constraint effect imposed by a crystalline framework, as previously observed for **COF$_{bpyMn}$**, thus resulting in the partial formation of a detrimental dimeric resting state. This study supports a COF effect on the electrocatalytic activity.

■ ASSOCIATED CONTENT

Supporting Information

The Supporting Information is available free of charge at https://pubs.acs.org/doi/10.1021/acsaem.3c03117.

Additional experimental details, materials, and methods; photographs of the experimental setup; and NMR, PXRD, BET, ICP-OES, IR, and CV characterization (PDF)

■ AUTHOR INFORMATION

Corresponding Author

Julio Lloret-Fillol − *Institute of Chemical Research of Catalonia (ICIQ), The Barcelona Institute of Science and Technology, Tarragona 43007, Spain; Catalan Institution for Research and Advanced Studies (ICREA), Barcelona 08010, Spain;* orcid.org/0000-0002-4240-9512; Email: jlloret@iciq.es

Authors

Geyla C. Dubed Bandomo − *Institute of Chemical Research of Catalonia (ICIQ), The Barcelona Institute of Science and Technology, Tarragona 43007, Spain*

Federico Franco − *Institute of Chemical Research of Catalonia (ICIQ), The Barcelona Institute of Science and Technology, Tarragona 43007, Spain*

Changwei Liu − *Institute of Chemical Research of Catalonia (ICIQ), The Barcelona Institute of Science and Technology, Tarragona 43007, Spain*

Suvendu Sekhar Mondal − *Institute of Chemical Research of Catalonia (ICIQ), The Barcelona Institute of Science and Technology, Tarragona 43007, Spain*

Angelo Gallo − *Dipartimento di Chimica e Centro di Eccellenza NIS, Università di Torino, Torino 10125, Italy;* orcid.org/0000-0001-9778-4822

Carlo Nervi − *Dipartimento di Chimica e Centro di Eccellenza NIS, Università di Torino, Torino 10125, Italy;* orcid.org/0000-0002-3712-7369

Complete contact information is available at: https://pubs.acs.org/10.1021/acsaem.3c03117

Notes

The authors declare no competing financial interest.

Part of the research herein is associated with the Dubed Bandomo, G. C. Development and Mechanistic Study of Single Sites in 2D-Covalent Organic Frameworks for CO_2 Electroreduction. Ph.D. Dissertation, Universidad Roviri I Virgili, Tarragona, 2022.

■ ACKNOWLEDGMENTS

The authors acknowledge the financial support of the ICIQ Foundation, the CERCA Program/Generalitat de Catalunya, MICINN through Severo Ochoa Excellence Accreditation 2020−2023 (CEX2019-000925-S, MIC/AEI), the European Research Foundation for H2020 project ERC-2015-CoG GREEN-LIGHT_REDCAT 648304 (J.L.-F.), AGAUR (2021 SGR 01260), and MICINN (PID2019-110050RB-I00, J.L-F.; PID2022-140142OB-I00, PDC2022-133451-I00, J.L.-F.) and "la Fundación Ramón Areces" (ElectroFuel).

■ REFERENCES

(1) Fernández, S.; Dubed Bandomo, G. C.; Lloret-Fillol, J. Recent advances in electrocatalytic CO2 reduction with molecular complexes. In *Recent Highlights II*; Advances in Inorganic Chemistry; Academic Press, 2022.

(2) Dubed Bandomo, G. C.; Mondal, S. S.; Franco, F.; Bucci, A.; Martin-Diaconescu, V.; Ortuño, M. A.; van Langevelde, P. H.; Shafir, A.; López, N.; Lloret-Fillol, J. Mechanically Constrained Catalytic Mn(CO)3Br Single Sites in a Two-Dimensional Covalent Organic Framework for CO2 Electroreduction in H2O. *ACS Catal.* **2021**, *11* (12), 7210−7222.

(3) Cheung, P. L.; Lee, S. K.; Kubiak, C. P. Facile Solvent-Free Synthesis of Thin Iron Porphyrin COFs on Carbon Cloth Electrodes for CO2 Reduction. *Chem. Mater.* **2019**, *31* (6), 1908−1919.

(4) Hod, I.; Sampson, M. D.; Deria, P.; Kubiak, C. P.; Farha, O. K.; Hupp, J. T. Fe-Porphyrin-Based Metal-Organic Framework Films as High-Surface Concentration, Heterogeneous Catalysts for Electrochemical Reduction of CO2. *ACS Catal.* **2015**, *5* (11), 6302−6309.

(5) Waller, P. J.; Gándara, F.; Yaghi, O. M. Chemistry of Covalent Organic Frameworks. *Acc. Chem. Res.* **2015**, *48* (12), 3053−3063.

(6) Diercks, C. S.; Lin, S.; Kornienko, N.; Kapustin, E. A.; Nichols, E. M.; Zhu, C.; Zhao, Y.; Chang, C. J.; Yaghi, O. M. Reticular Electronic Tuning of Porphyrin Active Sites in Covalent Organic Frameworks for Electrocatalytic Carbon Dioxide Reduction. *J. Am. Chem. Soc.* **2018**, *140* (3), 1116−1122.

(7) Lin, S.; Diercks, C. S.; Zhang, Y.-B.; Kornienko, N.; Nichols, E. M.; Zhao, Y.; Paris, A. R.; Kim, D.; Yang, P.; Yaghi, O. M.; Chang, C. J. Covalent organic frameworks comprising cobalt porphyrins for catalytic CO2 reduction in water. *Science* **2015**, *349* (6253), 1208−1213.

(8) Kornienko, N.; Zhao, Y.; Kley, C. S.; Zhu, C.; Kim, D.; Lin, S.; Chang, C. J.; Yaghi, O. M.; Yang, P. Metal-organic frameworks for electrocatalytic reduction of carbon dioxide. *J. Am. Chem. Soc.* **2015**, *137* (44), 14129−14135.

(9) Nie, W.; Tarnopol, D. E.; McCrory, C. C. L. Enhancing a Molecular Electrocatalyst's Activity for CO2 Reduction by Simultaneously Modulating Three Substituent Effects. *J. Am. Chem. Soc.* **2021**, *143* (10), 3764−3778.

(10) Gopalakrishnan, V. N.; Becerra, J.; Pena, E. F.; Sakar, M.; Béland, F.; Do, T.-O. Porphyrin and single atom featured reticular materials: recent advances and future perspective of solar-driven CO2 reduction. *Green Chem.* **2021**, *23* (21), 8332−8360.

(11) Grammatico, D.; Bagnall, A. J.; Riccardi, L.; Fontecave, M.; Su, B.-L.; Billon, L. Heterogenised Molecular Catalysts for Sustainable Electrochemical CO2 Reduction. *Angew. Chem., Int. Ed.* **2022**, *61* (38), No. e202206399.

(12) Boutin, E.; Merakeb, L.; Ma, B.; Boudy, B.; Wang, M.; Bonin, J.; Anxolabéhère-Mallart, E.; Robert, M. Molecular catalysis of CO2 reduction: recent advances and perspectives in electrochemical and light-driven processes with selected Fe, Ni and Co aza macrocyclic and polypyridine complexes. *Chem. Soc. Rev.* **2020**, *49* (16), 5772−5809.

(13) Baldwin, L. A.; Crowe, J. W.; Pyles, D. A.; McGrier, P. L. Metalation of a Mesoporous Three-Dimensional Covalent Organic Framework. *J. Am. Chem. Soc.* **2016**, *138* (46), 15134−15137.

(14) Ascherl, L.; Sick, T.; Margraf, J. T.; Lapidus, S. H.; Calik, M.; Hettstedt, C.; Karaghiosoff, K.; Döblinger, M.; Clark, T.; Chapman, K. W.; Auras, F.; Bein, T. Molecular docking sites designed for the generation of highly crystalline covalent organic frameworks. *Nat. Chem.* **2016**, *8* (4), 310−316.

(15) El-Kaderi, H. M.; Hunt, J. R.; Mendoza-Cortés, J. L.; Côté, A. P.; Taylor, R. E.; O'Keeffe, M.; Yaghi, O. M. Designed synthesis of 3D covalent organic frameworks. *Science* **2007**, *316* (5822), 268−272.

(16) Ding, S.-Y.; Gao, J.; Wang, Q.; Zhang, Y.; Song, W.-G.; Su, C.-Y.; Wang, W. Construction of Covalent Organic Framework for Catalysis: Pd/COF-LZU1 in Suzuki-Miyaura Coupling Reaction. *J. Am. Chem. Soc.* **2011**, *133* (49), 19816−19822.

(17) Doonan, C. J.; Tranchemontagne, D. J.; Glover, T. G.; Hunt, J. R.; Yaghi, O. M. Exceptional ammonia uptake by a covalent organic framework. *Nat. Chem.* **2010**, *2* (3), 235−238.

(18) Ngo, K. T.; McKinnon, M.; Mahanti, B.; Narayanan, R.; Grills, D. C.; Ertem, M. Z.; Rochford, J. Turning on the Protonation-First Pathway for Electrocatalytic CO2 Reduction by Manganese Bipyridyl Tricarbonyl Complexes. *J. Am. Chem. Soc.* **2017**, *139* (7), 2604−2618.

(19) Sampson, M. D.; Nguyen, A. D.; Grice, K. A.; Moore, C. E.; Rheingold, A. L.; Kubiak, C. P. Manganese Catalysts with Bulky Bipyridine Ligands for the Electrocatalytic Reduction of Carbon Dioxide: Eliminating Dimerization and Altering Catalysis. *J. Am. Chem. Soc.* **2014**, *136* (14), 5460−5471.
(20) Pakhira, S. Rotational dynamics of the organic bridging linkers in metal-organic frameworks and their substituent effects on the rotational energy barrier. *RSC Adv.* **2019**, *9* (65), 38137−38147.
(21) Pakhira, S.; Mendoza-Cortes, J. L. Quantum Nature in the Interaction of Molecular Hydrogen with Porous Materials: Implications for Practical Hydrogen Storage. *J. Phys. Chem. C* **2020**, *124* (11), 6454−6460.
(22) Pakhira, S.; Mendoza-Cortes, J. L. Tuning the Dirac Cone of Bilayer and Bulk Structure Graphene by Intercalating First Row Transition Metals Using First-Principles Calculations. *J. Phys. Chem. C* **2018**, *122* (9), 4768−4782.
(23) Pakhira, S.; Lucht, K. P.; Mendoza-Cortes, J. L. Dirac cone in two dimensional bilayer graphene by intercalation with V, Nb, and Ta transition metals. *J. Chem. Phys.* **2018**, *148* (6), 064707.
(24) Nguyen, H. L. Reticular design and crystal structure determination of covalent organic frameworks. *Chem. Sci.* **2021**, *12* (25), 8632−8647.
(25) Zhang, B.; Mao, H.; Matheu, R.; Reimer, J. A.; Alshmimri, S. A.; Alshihri, S.; Yaghi, O. M. Reticular Synthesis of Multinary Covalent Organic Frameworks. *J. Am. Chem. Soc.* **2019**, *141* (29), 11420−11424.
(26) Liu, X.; Li, J.; Gui, B.; Lin, G.; Fu, Q.; Yin, S.; Liu, X.; Sun, J.; Wang, C. A Crystalline Three-Dimensional Covalent Organic Framework with Flexible Building Blocks. *J. Am. Chem. Soc.* **2021**, *143* (4), 2123−2129.
(27) Jiang, H.; Alezi, D.; Eddaoudi, M. A reticular chemistry guide for the design of periodic solids. *Nat. Rev. Mater.* **2021**, *6* (6), 466−487.
(28) Hu, J.; Gupta, S. K.; Ozdemir, J.; Beyzavi, H. Applications of Dynamic Covalent Chemistry Concept toward Tailored Covalent Organic Framework Nanomaterials: A Review. *ACS Appl. Nano Mater.* **2020**, *3* (7), 6239−6269.
(29) Biswal, B. P.; Chandra, S.; Kandambeth, S.; Lukose, B.; Heine, T.; Banerjee, R. Mechanochemical Synthesis of Chemically Stable Isoreticular Covalent Organic Frameworks. *J. Am. Chem. Soc.* **2013**, *135* (14), 5328−5331.
(30) Cui, X.; Lei, S.; Wang, A. C.; Gao, L.; Zhang, Q.; Yang, Y.; Lin, Z. Emerging covalent organic frameworks tailored materials for electrocatalysis. *Nano Energy* **2020**, *70*, 104525.
(31) Dong, J.; Wang, Y.; Liu, G.; Cheng, Y.; Zhao, D. Isoreticular covalent organic frameworks for hydrocarbon uptake and separation: the important role of monomer planarity. *CrystEngComm* **2017**, *19* (33), 4899−4904.
(32) Lin, C.-Y.; Zhang, D.; Zhao, Z.; Xia, Z. Covalent Organic Framework Electrocatalysts for Clean Energy Conversion. *Adv. Mater.* **2018**, *30* (5), 1703646.
(33) Lyle, S. J.; Waller, P. J.; Yaghi, O. M. Covalent Organic Frameworks: Organic Chemistry Extended into Two and Three Dimensions. *Trends Chem.* **2019**, *1* (2), 172−184.
(34) Lei, K.; Yu Xia, B. Electrocatalytic CO2 Reduction: from Discrete Molecular Catalysts to Their Integrated Catalytic Materials. *Chem. - Eur. J.* **2022**, *28* (30), No. e202200141.
(35) Takeda, H.; Cometto, C.; Ishitani, O.; Robert, M. Electrons, Photons, Protons and Earth-Abundant Metal Complexes for Molecular Catalysis of CO2 Reduction. *ACS Catal.* **2017**, *7* (1), 70−88.
(36) Costentin, C.; Robert, M.; Savéant, J. M. Catalysis of the electrochemical reduction of carbon dioxide. *Chem. Soc. Rev.* **2013**, *42* (6), 2423−2436.
(37) Wang, J.; Huang, X.; Xi, S.; Xu, H.; Wang, X. Axial Modification of Cobalt Complexes on Heterogeneous Surface with Enhanced Electron Transfer for Carbon Dioxide Reduction. *Angew. Chem., Int. Ed.* **2020**, *59* (43), 19162−19167.
(38) Wang, J.; Huang, X.; Xi, S.; Lee, J. M.; Wang, C.; Du, Y.; Wang, X. Linkage Effect in the Heterogenization of Cobalt Complexes by Doped Graphene for Electrocatalytic CO2 Reduction. *Angew. Chem., Int. Ed.* **2019**, *58* (38), 13532−13539.
(39) Popov, D. A.; Luna, J. M.; Orchanian, N. M.; Haiges, R.; Downes, C. A.; Marinescu, S. C. A 2,2′-bipyridine-containing covalent organic framework bearing rhenium(i) tricarbonyl moieties for CO2 reduction. *Dalton Trans.* **2018**, *47* (48), 17450−17460.
(40) Aiyappa, H. B.; Thote, J.; Shinde, D. B.; Banerjee, R.; Kurungot, S. Cobalt-Modified Covalent Organic Framework as a Robust Water Oxidation Electrocatalyst. *Chem. Mater.* **2016**, *28* (12), 4375−4379.
(41) Johnson, E. M.; Haiges, R.; Marinescu, S. C. Covalent-Organic Frameworks Composed of Rhenium Bipyridine and Metal Porphyrins: Designing Heterobimetallic Frameworks with Two Distinct Metal Sites. *ACS Appl. Mater. Interfaces* **2018**, *10* (44), 37919−37927.
(42) López-Magano, A.; Ortín-Rubio, B.; Imaz, I.; Maspoch, D.; Alemán, J.; Mas-Ballesté, R. Photoredox Heterobimetallic Dual Catalysis Using Engineered Covalent Organic Frameworks. *ACS Catal.* **2021**, *11* (19), 12344−12354.
(43) Feng, X.; Ding, X.; Jiang, D. Covalent organic frameworks. *Chem. Soc. Rev.* **2012**, *41* (18), 6010−6022.
(44) Auras, F.; Ascherl, L.; Hakimioun, A. H.; Margraf, J. T.; Hanusch, F. C.; Reuter, S.; Bessinger, D.; Döblinger, M.; Hettstedt, C.; Karaghiosoff, K.; Herbert, S.; Knochel, P.; Clark, T.; Bein, T. Synchronized Offset Stacking: A Concept for Growing Large-Domain and Highly Crystalline 2D Covalent Organic Frameworks. *J. Am. Chem. Soc.* **2016**, *138* (51), 16703−16710.
(45) Bisbey, R. P.; Dichtel, W. R. Covalent Organic Frameworks as a Platform for Multidimensional Polymerization. *ACS Cent. Sci.* **2017**, *3* (6), 533−543.
(46) Da, H.-J.; Yang, C.-X.; Qian, H.-L.; Yan, X.-P. A knot-linker planarity control strategy for constructing highly crystalline cationic covalent organic frameworks: decoding the effect of crystallinity on adsorption performance. *J. Mater. Chem. A* **2020**, *8* (25), 12657−12664.
(47) Huang, X.; Sun, C.; Feng, X. Crystallinity and stability of covalent organic frameworks. *Sci. China: Chem.* **2020**, *63* (10), 1367−1390.
(48) Walsh, J. J.; Forster, M.; Smith, C. L.; Neri, G.; Potter, R. J.; Cowan, A. J. Directing the mechanism of CO2 reduction by a Mn catalyst through surface immobilization. *Phys. Chem. Chem. Phys.* **2018**, *20* (10), 6811−6816.
(49) Reuillard, B.; Ly, K. H.; Rosser, T. E.; Kuehnel, M. F.; Zebger, I.; Reisner, E. Tuning Product Selectivity for Aqueous CO2 Reduction with a Mn(bipyridine)-pyrene Catalyst Immobilized on a Carbon Nanotube Electrode. *J. Am. Chem. Soc.* **2017**, *139* (41), 14425−14435.
(50) Rotundo, L.; Filippi, J.; Gobetto, R.; Miller, H. A.; Rocca, R.; Nervi, C.; Vizza, F. Electrochemical CO2 reduction in water at carbon cloth electrodes functionalized with a fac-Mn(apbpy)(CO)3Br complex. *Chem. Commun.* **2019**, *55* (6), 775−777.
(51) Filippi, J.; Rotundo, L.; Gobetto, R.; Miller, H. A.; Nervi, C.; Lavacchi, A.; Vizza, F. Turning manganese into gold: Efficient electrochemical CO2 reduction by a fac-Mn(apbpy)(CO)3Br complex in a gas-liquid interface flow cell. *Chem. Eng. J.* **2021**, *416*, 129050.
(52) Chen, X.; Addicoat, M.; Irle, S.; Nagai, A.; Jiang, D. Control of Crystallinity and Porosity of Covalent Organic Frameworks by Managing Interlayer Interactions Based on Self-Complementary π-Electronic Force. *J. Am. Chem. Soc.* **2013**, *135* (2), 546−549.
(53) Jin, S.; Ding, X.; Feng, X.; Supur, M.; Furukawa, K.; Takahashi, S.; Addicoat, M.; El-Khouly, M. E.; Nakamura, T.; Irle, S.; Fukuzumi, S.; Nagai, A.; Jiang, D. Charge dynamics in a donor-acceptor covalent organic framework with periodically ordered bicontinuous heterojunctions. *Angew. Chem., Int. Ed.* **2013**, *52* (7), 2017−2021.
(54) Rosser, T. E.; Windle, C. D.; Reisner, E. Electrocatalytic and Solar-Driven CO2 Reduction to CO with a Molecular Manganese Catalyst Immobilized on Mesoporous TiO2. *Angew. Chem., Int. Ed.* **2016**, *55* (26), 7388−7392.
(55) Franco, F.; Cometto, C.; Nencini, L.; Barolo, C.; Sordello, F.; Minero, C.; Fiedler, J.; Robert, M.; Gobetto, R.; Nervi, C. Local Proton Source in Electrocatalytic CO2 Reduction with [Mn(bpy-R)(CO)3Br] Complexes. *Chem. - Eur. J.* **2017**, *23* (20), 4782−4793.
(56) McKinnon, M.; Belkina, V.; Ngo, K. T.; Ertem, M. Z.; Grills, D. C.; Rochford, J. An Investigation of Electrocatalytic CO2 Reduction

Using a Manganese Tricarbonyl Biquinoline Complex. *Front. Chem.* **2019**, *7*, 628.
(57) Grills, D. C.; Ertem, M. Z.; McKinnon, M.; Ngo, K. T.; Rochford, J. Mechanistic aspects of CO2 reduction catalysis with manganese-based molecular catalysts. *Coord. Chem. Rev.* **2018**, *374*, 173−217.
(58) Rønne, M. H.; Madsen, M. R.; Skrydstrup, T.; Pedersen, S. U.; Daasbjerg, K. Mechanistic Elucidation of Dimer Formation and Strategies for Its Suppression in Electrochemical Reduction of Fac-Mn(bpy)(CO)3Br. *ChemElectroChem* **2021**, *8* (11), 2108−2114.